Closed-loop recruitment of striatal parvalbumin interneurons prevents the onset of compulsive behaviors

Authors

Mondragon-Gonzalez LS[1*], Schreiweis C[1*], Burguière E[1, §]

Author Affiliations & Addresses

[1]Sorbonne Université, Institut du Cerveau - Paris Brain Institute - ICM, Inserm, CNRS, AP-HP, Hôpital de la Pitié Salpêtrière, Paris, France

* These authors contributed equally to the publication.

§ Corresponding author

Corresponding author

Eric Burguière, PhD

Email: eric.burguiere@icm-institute.org

Phone: +33-1.57.27.44.25

ABSTRACT

A prominent electrophysiological feature of compulsive behaviours is striatal hyperactivity; but its underlying dysfunctional cellular mechanisms still need to be characterized. Within the striatum, parvalbumin-positive interneurons (PVI) exert a powerful feedforward inhibition essential for the regulation of striatal activity. To investigate the potential implication of striatal PVI in aberrant repetitive behaviors, we used the Sapap3 mutant mice which exhibit compulsive-like behaviours characterized by excessive self-grooming. When striatal PVI in the centromedial striatum of Sapap3 mice were we optogenetically activated, we first showed that the number of compulsive-like events were greatly reduced. To investigate further the critical time-window when striatal PVI needed to be recruited for the behavioural regulation of compulsive-like grooming, we then designed a novel closed-loop stimulation pipeline. We identified a transient 1-4 Hz oscillations in the orbitofrontal cortex that temporally predicted grooming onsets. Exploiting this delta band signal as a biomarker, we were able to provide on-demand stimulation of striatal PVI shortly before predicted grooming events. This targeted closed-loop optogenetics approach greatly reduced grooming events and demonstrated that the recruitment of striatal PVI regulated the initiations of compulsive-like behaviours.

INTRODUCTION

Compulsive behaviours consist of pathological repetitive behaviours executed despite negative consequences. They are a core feature of various neuropsychiatric disorders, including obsessive-compulsive disorder (OCD). Increasing evidence in studies of neuropsychiatric disorders with repetitive behaviours points toward malfunctioning cortico-basal ganglia circuits, which are key players in the formation and regulation of actions[1,2]. In particular, altered fronto-striatal circuits, including orbito-frontal cortex (OFC) projecting to centro-medial striatum (CMS), have been observed in OCD patients[3,4] as well as in rodent models expressing pathological repetitive behaviours[5–7]. Striatal hyperactivity has surfaced as one of the prominent physiological characteristics during compulsive episodes[6–9], and reduction of striatal activity correlates with symptoms alleviation in OCD patients[10,11]. However, the neuronal abnormalities that underlie this striatal hyperactivity in compulsive behaviours and related disorders remain to be characterized. Under normal conditions, fast-spiking parvalbumin striatal interneurons (PVI) receive strong afferences from the cortex and regulate the activity of striatal medium spiny neurons (MSN) through a powerful feedforward inhibition given their earlier and low activation threshold relative to MSN[10,12–15]. These physiological properties have been proposed to orchestrate and tune MSN activity to adapt and regulate behavioural output[16–18]. Interestingly, post-mortem studies of patients and mouse models suffering from pathological repetitive behaviours have reported a consistent decrease in PVI density in medial striatal areas[19–22]. Together, this previous evidence suggests a crucial link between decreased PVI function and dysregulation of pathological repetitive behaviours, but a causal connection has been lacking to date. To study the contributions of PVI in regulating compulsive behaviours, we used the Sapap3$^{-/-}$ mouse model that displays both striatal hyperactivity and a decreased density of PVI in medial striatal areas[6,23]. To prove and temporally precisely define their role in the emergence of transient and spontaneous compulsive-like behaviours, we have established a closed-loop optogenetic approach by constructing a real-time responsive system, which could be triggered by detecting a reliable biomarker predictive of the symptom.

RESULTS

I. Recruitment of striatal parvalbumin-expressing interneurons alleviates compulsive-like behaviours

We bilaterally injected Sapap3$^{-/-}$ :: PV$^{Cre/Wt}$ (Sapap3-PVCre) mice (n=10) with a Cre-dependent adeno-associated viral vector expressing channelrhodopsin-2 (AAV5-hChR2(H134R)-mCherry) into the centro-medial striatum (CMS) (Fig. 1a,b). Bilateral implantation of optic fibers at the injection site allowed us to selectively recruit parvalbumin-positive fast-spiking interneurons (PVI) in the CMS (Fig. 1c, Extended Data Fig.1a) via a customized implant designed for simultaneous optogenetic neuromodulation and *in-vivo* electrophysiology (Extended Data Fig. 2). On three separate days, we videotaped naïve freely-moving Sapap3-PVCre mice while delivering optogenetic stimulation (5-ms pulses at 20 Hz, 10mW). The experimental paradigm consisted of a 10–15-minute habituation period, followed by ten alternating trials of 3 minutes

of active blue light stimulation (ON) and 3 minutes without blue light stimulation (OFF, Fig. 1d). During the PVI optogenetic activation periods, the Sapap3-PVCre mice exhibited a significant decrease of grooming bouts by 55.8% and of grooming duration by 46.25%, to levels comparable to wild-type baselines (Fig. 1e, f). This effect was consistent across trials (Fig. 1e, f upper panels) and sessions (Fig. 1e, f lower panels, Extended Data Fig. 3). On the contrary, under the same protocol, age-matched control groups including Sapap3-PVCre mice expressing a virus with a fluorescent reporter only (AAV5-mCherry) (n=6) and wild-types (Sapap3$^{+/+}$:: PV$^{Cre/wt}$) expressing hChR2-mCherry (n=5) did not significantly decrease their grooming activity during the blue light stimulation trials (Fig. 1e, f). To further understand the reduction of grooming activity upon optogenetic excitation of striatal PVI in Sapap3-PVCre expressing hChR2-mCherry, we looked at individual grooming bouts. We found that the average duration of individual grooming events was consistent between ON and OFF trials (Fig. 1g), pointing out that the overall decrease of grooming duration was due to a reduced number of grooming bout initiations. Our findings showed that selective stimulation of striatal PVI activity alleviates excessive self-grooming by reducing the number of grooming onsets and suggest their implication in the regulation of grooming initiations.

II. A transient lOFC delta band signature predicts compulsive-like grooming onsets.

To causally prove that striatal PVI recruitment is sufficient for GO regulation, we sought a predictive biomarker in order to drive their activity before GO. To this end, we focused on one of the most prominent candidate regions implicated in compulsive-like behaviours, the orbitofrontal cortex (OFC)[3,24–26]. Its rodent homolog has been shown to play a crucial neurophysiological role also in the Sapap3$^{-/-}$ mouse model of compulsive-like behaviours[6,9,27,28]. We investigated grooming-related local field potential (LFP) activity in freely moving Sapap3-PVCre mice (n=10) by performing *in-vivo* extracellular tetrode recordings in the lateral orbitofrontal cortex (lOFC). We manually annotated video frames of GO, which we defined as the first noticeable movement of front limbs engaging in a grooming event (Extended Data Fig. 4a). We selected grooming events with no preceding motor behaviours to exclude movement confounders. We contrasted the power spectral density of average pre-grooming activity (-1s to GO) with that of average resting activity (Fig. 2a). Despite the comparable stillness displayed by the animal during resting and pre-grooming states, their corresponding power spectrum distributions differed, particularly within the delta frequency band (1.5-3 Hz). This low-frequency band power in pre-grooming activity consistently increased until GO (Fig. 2b). This ramping effect was characterized by an average rising point approximately 1s before GO and an average maximal power around 2 Hz (Fig. 2c-e). The narrow temporal power increase in delta range frequency preceding GO was observed in individual Sapap3-PVCre mice (Extended Data Fig. 4b). As the average rising point occurred at approximately 1s prior to GO, this power increment embedded the predictive dimension required for driving PVI activity before GO using closed-loop neuromodulatory intervention. To that end, we developed a supervised learning method for the automatic processing of neural signals as they are acquired via multiple tetrodes and decomposed the raw signals into a small representative matrix of coefficients (Fig. 3a). Thus, this filter reduction step allowed us to train a light feedforward artificial neural network with an output layer of two outcomes,

one for pre-grooming events and the other for other behaviours (OB) such as scratching, rearing, walking, standing, and resting. The training datasets were extracted and shuffled from five one-hour recording sessions for each experimental animal on different days. For each animal, the detection of a pre-grooming activity was validated if the LFP activity recorded on at least 50% of the electrodes was classified as pre-grooming. This model allowed us to predict GO successfully in Sapap3$^{-/-}$ mice (n=5) with an average offline performance of 63.52% accuracy, 61.08% precision, 65.34% specificity, and 64.2% recall (Fig. 3b).

III. Closed-loop optogenetic stimulation of striatal PVI prevents grooming onset

Taking advantage of the real-time detection of LFP signal in the lOFC predicting grooming onset, we designed a closed-loop approach in Sapap3-PVCre mice expressing hChR2(H134R)-mCherry. In this approach, the real-time prediction of GO would trigger an optogenetic controller to deliver on-demand light stimulation bilaterally in the CMS to specifically recruit striatal PVI when GO is predicted (Fig. 4a). We designed a 3D-printed homemade headstage for this experimental paradigm that allowed us to implant tetrodes in the lOFC and optic fibers bilaterally in the CMS (Extended Data Fig.2 c-e). Similar to the continuous stimulation procedure, the experimental paradigm included a habituation stage of 10-15 minutes, followed by alternating 3 minute trials of 'Off', 'Closed-loop', and 'Yoked' stimulation (12 trials total) (Fig. 4b). During 'Off' trials, no stimulation was delivered. During 'Closed-loop' trials, grooming events were automatically predicted online, which triggered the delivery of blue light pulses for 4 seconds (5-ms pulses at 20Hz and 10mW). During 'Yoked' trials, the number of light stimulations equaled that of the immediately preceding ‘Closed-loop’ trial; however they were randomly assigned across the 3 minutes. This protocol was repeated on three different days. We found that closed-loop optogenetic stimulation significantly reduced GO in Sapap3-PVCre mice (n=5) when compared to 'Off' and ‘Yoked’ trials (Fig. 4c). As in the continuous stimulation protocol, this effect was consistent across trials and sessions (Extended Data Fig. 5) and observed across all animals (Fig. 4c, bottom). The number of bouts and the grooming duration were reduced by 62.37% and 70.54%, respectively (Fig. 4d, e and Extended Data Fig. 6a). In line with results obtained in continuous optogenetic stimulation experiments, the character and duration of individual grooming sequences remained unaltered (Extended Data Fig. 6b). Finally, our ‘closed-loop’ approach was as efficient as ‘continuous’ stimulation protocol in terms of reducing the number of grooming bouts (Fig. 4d) and grooming duration (Fig. 4e), but with a tremendous reduction of stimulation time by 87.2% (Fig. 4f).

DISCUSSION

By combining optogenetic neuromodulation with a closed-loop stimulation protocol, we demonstrate in our study that the recruitment of striatal PVI prior to grooming onset was sufficient to regulate compulsive-like behaviours of the Sapap3$^{-/-}$ mice. Indeed, we first showed that continuous optogenetic stimulation of the PVI network in the centro-medial striatum had an immediate effect in reducing the compulsive-like number of grooming events

in Sapap3$^{-/-}$ mice to that of matched wildtype controls. Next, when seeking after a neurophysiological predictor of compulsive-like events to define the critical period for the recruitment of the PVI network, we detected an increase in the spectral power of the delta band activity in the lateral OFC, which shortly and consistently preceded grooming onset. To our knowledge, this is the first report of transient LFP events in the OFC that predict compulsive-like grooming episodes. Using this predictor, we designed a closed-loop approach based on an innovative supervised machine learning protocol to recruit the striatal PVI network prior to compulsive-like grooming onset. With this closed-loop system, we showed that brief optogenetic PVI excitation upon grooming event prediction was sufficient to abort their occurrence and reduce compulsive-like behaviours in Sapap3$^{-/-}$ mice. Taken together, we believe that these results will be valuable in understanding the biological mechanisms underlying repetitive behaviours and also open new ways of designing therapeutical approaches for treating pathological repetitive behaviours.

Indeed, our results showed that striatal PVI are essential in preventing the onset of compulsive-like behaviours in Sapap3$^{-/-}$ mice, presumably by inhibiting hyper-active MSN projection neurons[6,19]. These observations align with previous studies that showed the implication of striatal PVI during suppression of prepotent inappropriate actions, regulation of choice execution, or generation of complex motor sequences[29–31]. The crucial role of striatal PVI in regulating compulsive-like grooming in the Sapap3$^{-/-}$ mice is also supported by recent studies describing abnormal synaptic properties of striatal PVI in this animal model[32] as well as by observations in other mouse models suffering from pathological repetitive behaviours where abnormally low PVI density in striatal areas was observed[22]. Our study proposes that the fine temporal recruitment of striatal PVI shortly before the onset of compulsive-like behaviours is crucial to regulate their initiation.

However, the mechanistic process by which the striatal PVI network could be recruited still needs to be characterized. Interestingly, two recent studies have shown that the emergence of delta oscillations in the prefrontal cortex coincides with the recruitment of pyramidal cell assemblies[33,34]. In the context of our study, it would be interesting to investigate whether such recruitment of pyramidal cells can occur through OFC delta oscillations preceding grooming behaviours. Consequently, this cortical drive would allow for the temporally adjusted recruitment of the striatal PVI network to regulate the expression of grooming behaviours. This hypothesis could be supported by the fact that Sapap3$^{-/-}$ mice display a decreased spectral power in the low-frequency band in the OFC, including the delta range, compared to wildtype mice[27]. Thus, a lower LFP delta band in the OFC of Sapap3$^{-/-}$ mice may underlie impaired recruitment of downstream striatal PVI network and thus a decreased regulation of compulsive-like behaviours. Our findings also echo a recent study in OCD patients implanted with recording-capable DBS devices; the authors showed that LFP signals recorded in the striatum were co-occuring with OCD symptoms and detected a signature of interest in the delta-band, as we observed in our study[35].

Our findings also call for testing potential therapeutical strategies where striatal PVI could be specifically targeted in pathologies with compulsive behaviours. For instance, electrical deep brain stimulation (DBS) protocols have been used in severe OCD patients with good but limited efficiency in reducing symptoms while targeting different brain structures along basal ganglia circuits [36–38]. As continuous electrical DBS does not differentiate between different neuronal populations, this therapeutical approach may be improved by adapting stimulation protocols in order to reach cell-type specificity. Such possibility has been confirmed in a recent study

where the authors demonstrated that they could specifically recruit PVI in the globus pallidus by using brief bursts of electrical stimulation[39]. Building upon these findings and our results, it will be interesting to test such optimized DBS procedures in the context of pathological repetitive behaviours in order to specifically recruit striatal PVI.

Another interesting aspect of our study was the development of an innovative supervised machine learning approach to automatically provide optogenetic stimulation with context-specificity. The technical innovation of our approach for continuous processing of electrophysiological brain signals was to develop a coefficient decomposition stage to drastically reduce the number of variables to work with, the following stages in signal processing require less computing power and allow for simpler architectures that could be implemented in general-purpose computers, as we did in our experiments. We believe that this methodology would be of great interest for exploiting neurophysiological signals in a real-time manner such as adaptive DBS and more generally in brain-machine interface processes[40,41]. Our closed-loop approach was necessary to prove that recruitment of striatal PVI was crucial at the onset of the grooming while significantly reducing the stimulation time by 87%. However, it would be interesting to investigate further the long-term effects of targeted closed-loop modulation, such as a potential lasting reduction of compulsive-like behaviours as already observed with patterned neuromodulation protocols[39]. Additionally, the predictive approach implemented may be useful in further experiments as a platform to explore in a closed-loop manner other brain targets for therapeutic purposes.

FIGURES

FIGURE 1.

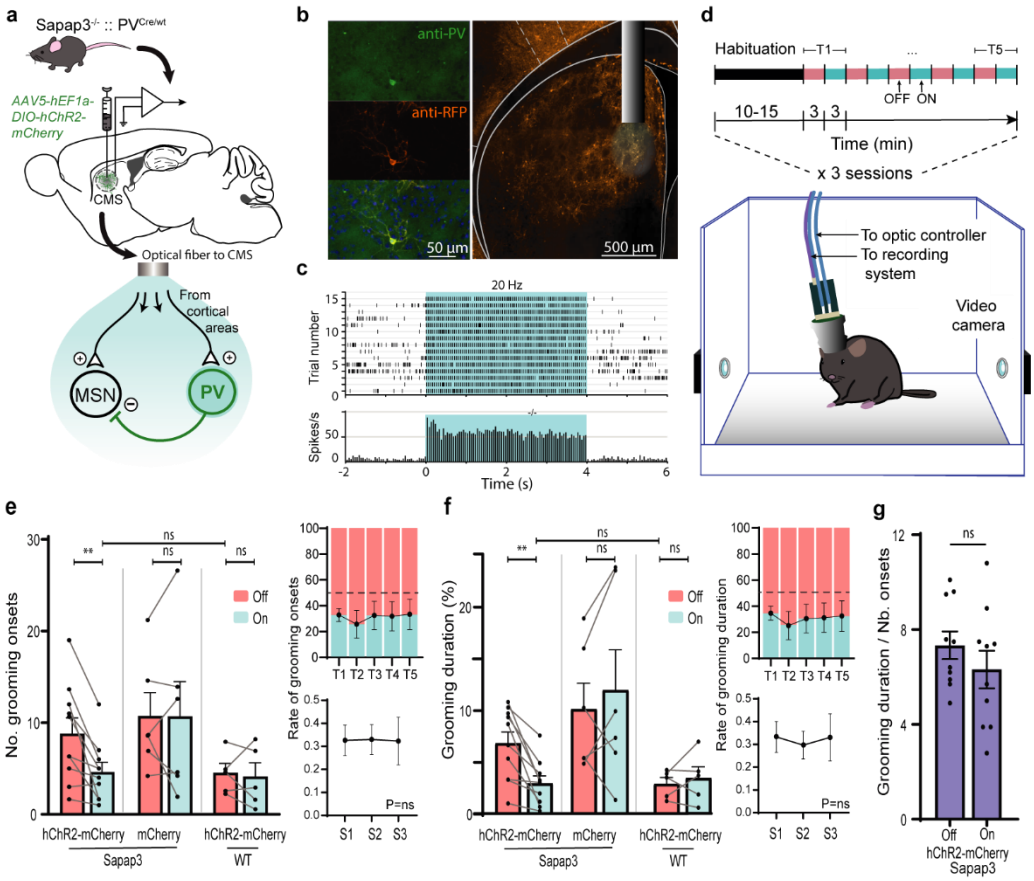

Figure1. Optogenetic activation of centro-medial striatal parvalbumin-positive interneurons reduces compulsive-like behaviour in Sapap3$^{-/-}$ mice. (**a**) Schematic illustration of the experimental preparation combining *in-vivo* multi-electrode recordings and optogenetic manipulation with a simplified model of the targeted striatal parvalbumin-positive interneuron (PVI) microcircuit. PVI are excited by blue light (465 nm) via bilateral optical fibers implanted in the CMS. (**b**) *Post-hoc* histological confirmation of selective striatal PV-expressing cells (anti-PV immunostaining, green). (**c**) Acute extracellular recordings during resting periods to confirm optogenetic activation effect of PVI in CMS as shown by the exemplar spike raster (top) and peri-stimulus time histogram (PSTH, below) from a PVI exhibiting rapid light-evoked excitation during 15 repetitions (bin width 50 ms). The blue rectangle marks the LED illumination period (4s). (**d**) Experimental setup and optogenetic stimulation paradigm. The blue bars denote the duration of bilateral continuous optical stimulation (20 Hz, 5-ms light pulses, 10 mW). (**e**) Optogenetic activation of CMS PV interneurons reduces grooming bout initialisation only in the Sapap3-PVCre mice group (n= 10, Wilcoxon matched pairs test, W= 53, **P ≤ 0.01) to wild-type baseline grooming levels (Mann-Whitney test, U=24, P=0.93) and, consequently, decreases the (**f**) total percentage of time spent in grooming (n= 10, Wilcoxon matched pairs test, W= 55, **P ≤ 0.01) in the same way (P=0.20, U=22, Mann-Whitney test). This reduction in grooming activity is not observed in the control groups, including Sapap3$^{-/-}$ injected with a control virus (n=5) and wild-type mice injected with a virus carrying the excitatory opsin (n=5). (**g**) The optogenetics stimulation did not affect the average duration of individual grooming events. Error bars represent mean ±SEM.

FIGURE 2.

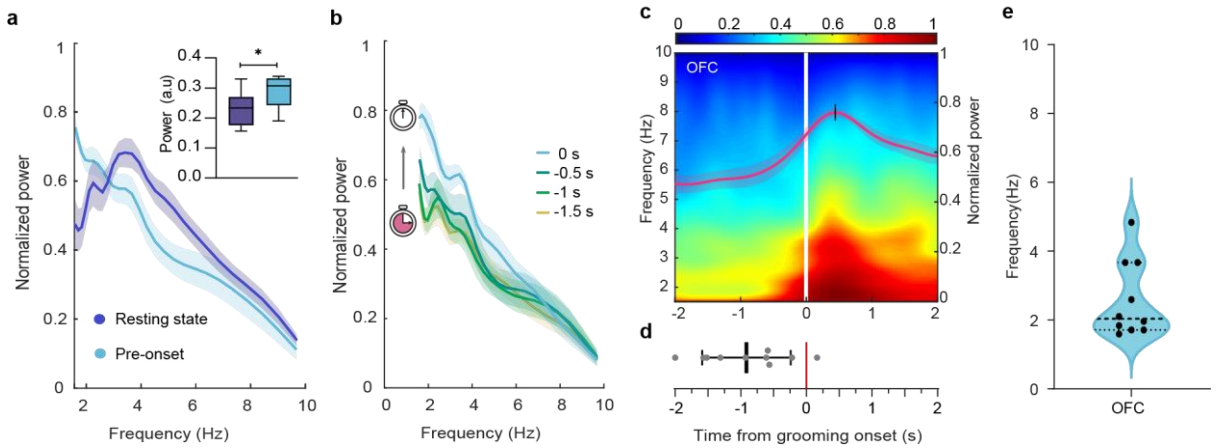

Figure 2. Orbitofrontal cortex low-frequency LFP signature predicts grooming onset in Sapap3$^{-/-}$ mice. (**a**) Power spectral density of average OFC LFPs recorded during one-second periods of pre-grooming onsets and resting-state periods. (Insert) Averaged OFC 1.5-3 Hz power for 15 pre-grooming events and 15 resting-states for each Sapap3$^{-/-}$ mouse. Whiskers represent minimum and maximum values (**P ≤ 0.01, Wilcoxon matched pairs test). (**b**) Time course of the average power spectral density recorded in the OFC in incrementing time windows of 500ms from -2s prior to grooming onset. (**c**) Average scalogram for the continuous wavelet transform of OFC activity in Sapap3$^{-/-}$ mice showing the increase in low-frequency power before GO. The vertical white line indicates GO. Warmer colors represent higher energy. The superimposed red trace represents the normalized power of the 1.5-4 Hz frequency band averaged across animals (right-hand y-axis). (**d**) Rising points for the time-frequency curve (1.5 – 4 Hz) for each Sapap3-/- mouse (mean = -0.91, SD=±0.67, min = -2, max=0.16). (**e**) Violin plot showing the distribution of frequencies at which the maximum power value is found within a 4s time range peri-GO (median= 2.03, skewness = 1.16, mean=2.57, SD=±1.11). N=10 Sapap3$^{-/-}$ mice.

FIGURE 3.

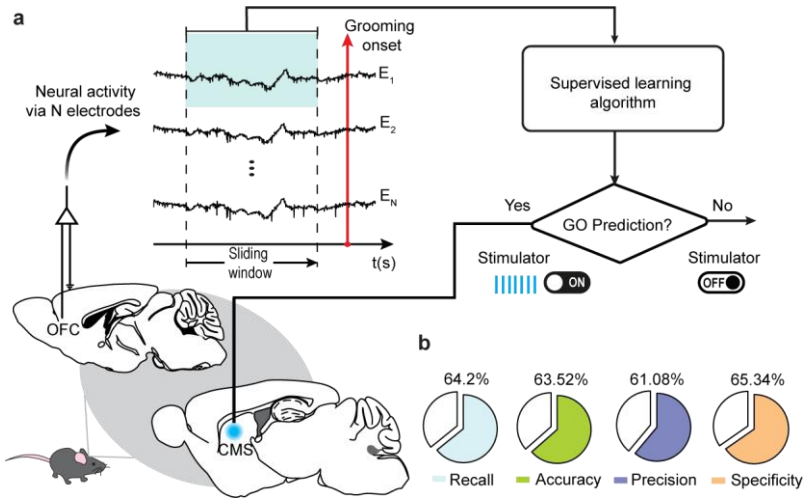

Figure 3. Orbitofrontal cortex low-frequency LFP signature predicts grooming onset in SAPAP3-KO mice. (a) Extracellular signals in the OFC are acquired through a chronic drive implant holding 32 recording channels. The signals are acquired at a sampling frequency of 20 kHz, and they are amplified and digitalised while the animal can freely behave. The LFP signals are processed to obtain low-frequency power band feature to train a supervised classification algorithm with an output layer with two neurons, one for pre-compulsive behaviour and the other for a collection of different types of behaviour. (**b**) Average performance of the algorithm in offline tests including accuracy (mean 63.52%, SD=±7.4), precision (mean= 61.08%, SD=±7.9), specificity (mean= 65.34%, SD=±27.6) and recall (mean=64.2%, SD=±25.9). N=5 Sapap3$^{-/-}$ mice.

FIGURE 4.

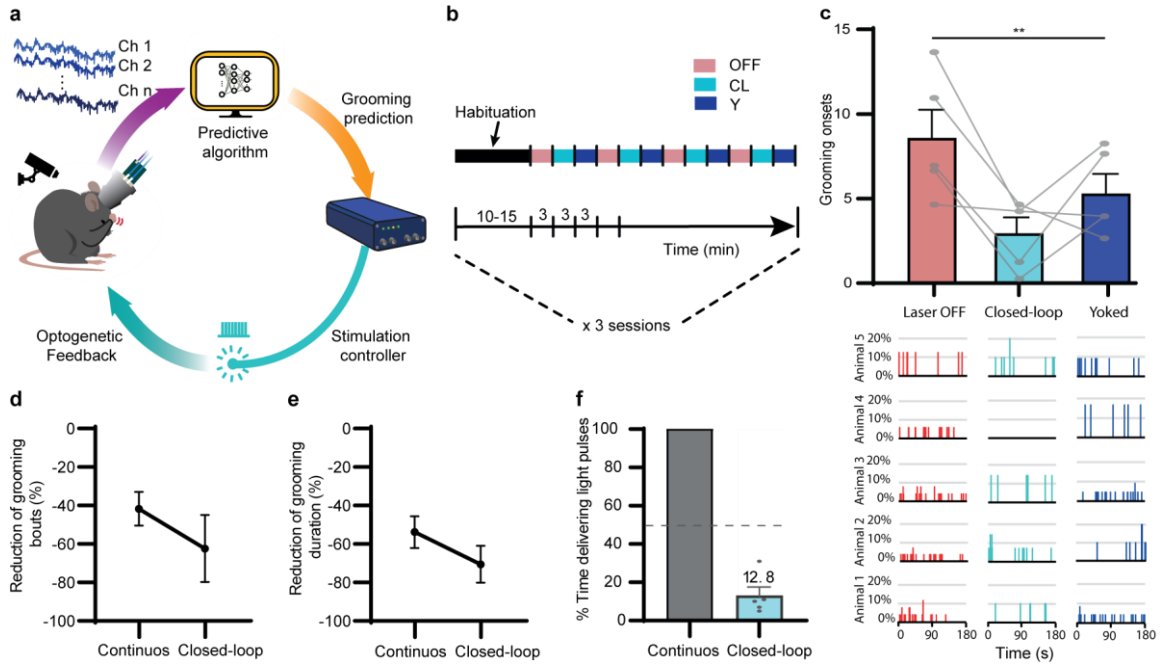

Figure 4. Closed-loop optogenetic intervention alleviates compulsive grooming. (a) Schematic illustration of the closed-loop experimental paradigm implemented for on-demand optogenetic intervention. Sapap3-PVCre mice were implanted for both neural activity acquisitions and light stimulation. The violet arrow indicates lOFC local field potentials acquired and digitalised at the mouse head-level. Based on online feature decomposition and reduction extracted from lOFC LFP signals and a supervised classification algorithm, a command signal (orange arrow) is sent to activate a stimulation controller to deliver light pulses of blue light during 4s. At the same time, animal behaviour is video recorded during the experiment. (**b**) Illustration of the closed-loop optogenetic stimulation protocol. (**c**) The average number of GO during the three different experimental conditions showed that there was a statistically significant trend of lower median GO within the closed-loop condition (Jonckheere-Terpstra test for non-parametric trend analysis for ordered alternatives from 'closed-loop', 'yoked' to 'laser-off' condition, T_{JT}= 2.32, **P ≤ 0.01, error bars represent mean ±SEM). The corresponding GO histogram displays the GO distribution across the experimental period for each Sapap3-PVCre mouse (down inset). (**d**) The averaged percentage of time the mice spent receiving optogenetic stimulation (mean=12.8%, SD=±10.45, minimum= 5, maximum = 31) shows a reduction of 87.2 % of the stimulation time compared to the continuous stimulation protocol. **(e)** Percentage of reduction in grooming bouts in continuous (mean= -41.72%, SE=±8.7) and closed-loop (mean= -62.37%, SE=±17.45) stimulation paradigms as well as (**f**) the resulting percentage in grooming duration reduction for continuous (mean=-(53.82%, SE=±8.18) and closed-loop condition (mean=-70.54, SE=±9.55). N=5 Sapap3-PVCre mice. Error bars represent mean ±SEM

EXTENDED FIGURE 1.

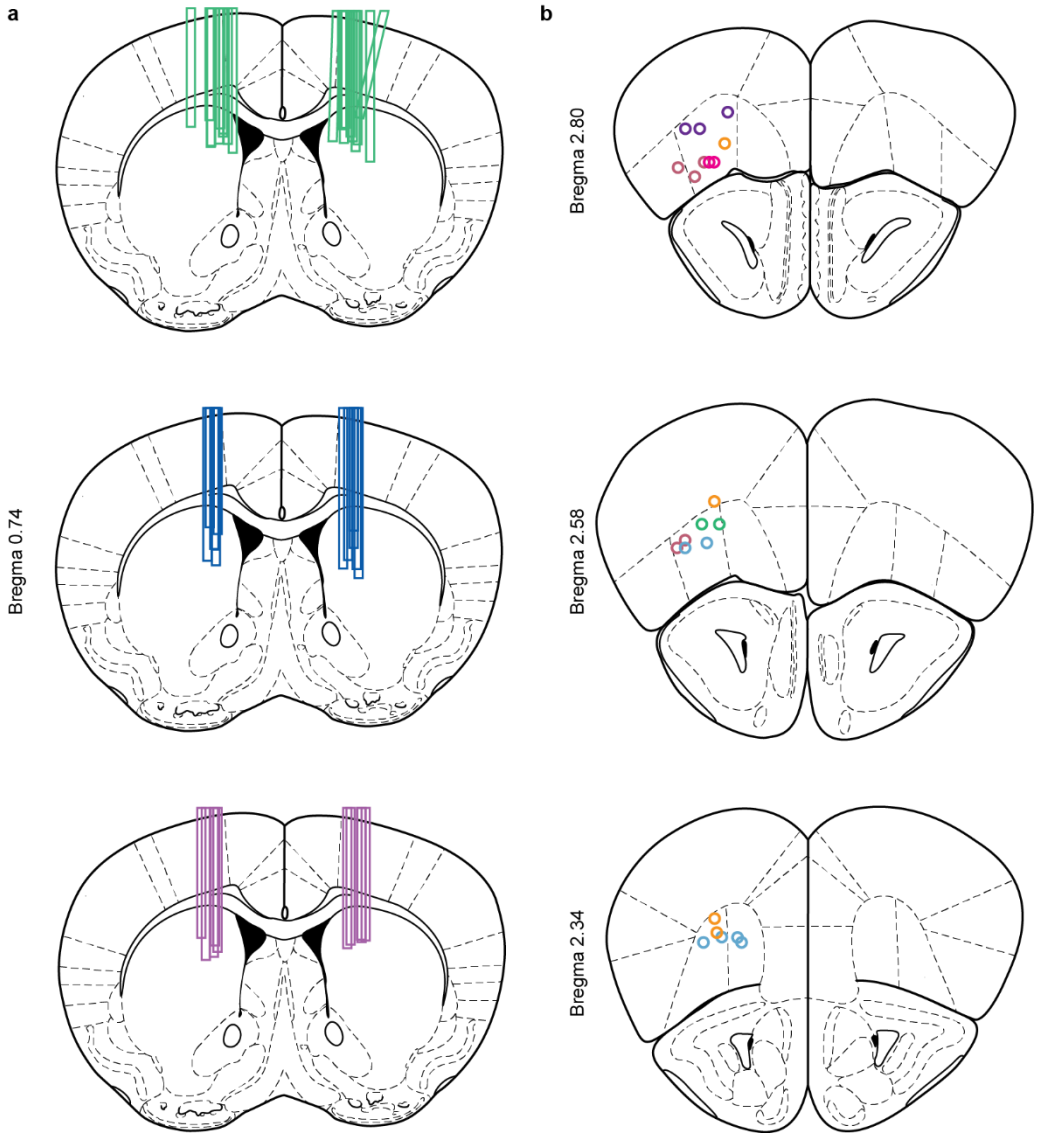

Extended Data Figure 1. *Post-hoc* histological confirmation of optic fiber and tetrode tip placements in the target regions CMS and lOFC. Specific reconstruction of the fiber tracks in the CMS (**a**) and electrophysiological recording sites in lOFC (**b**), mapped to the coronal sections of a mouse brain atlas (Paxinos, G. & Franklin, K. B. J., 2008). The location of each fiber tip was confirmed by comparing fiber tracks in histological coronal sections with measured fiber lengths of the detached implant after perfusion of the implanted animals. The location of each tetrode tip was determined based on electrolytic mark lesions in prefrontal coronal sections. CMS = centromedial striatum; lOFC = lateral orbitofrontal cortex.

EXTENDED FIGURE 2.

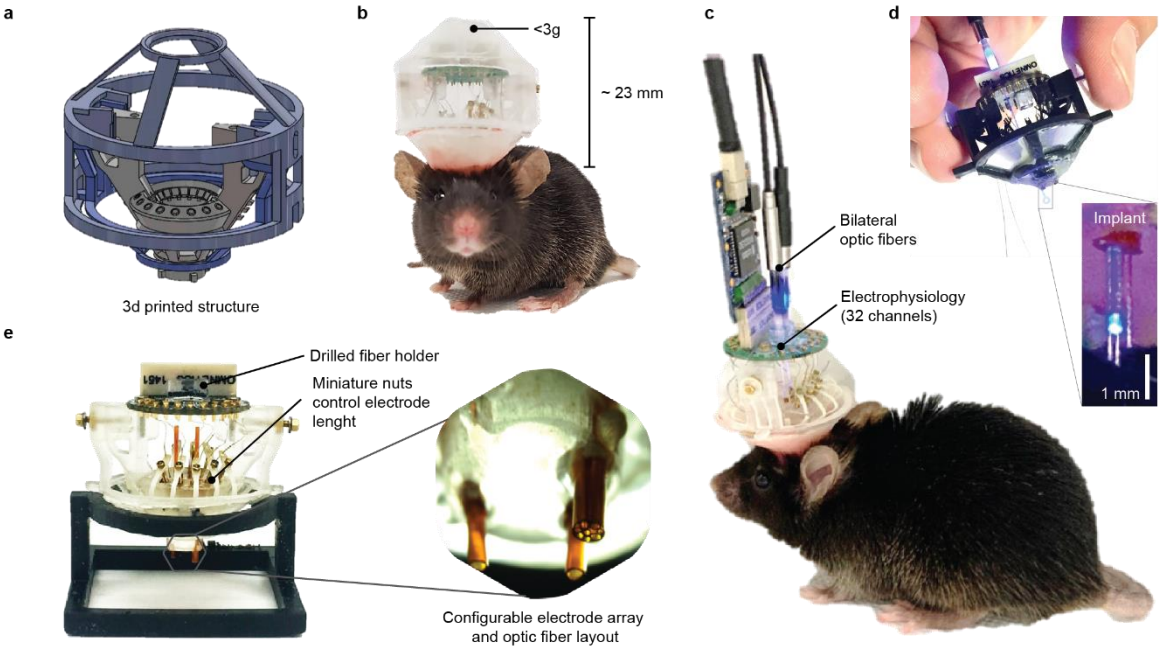

Extended Data Figure 2. Combined optic-fiber and electrophysiology implant for simultaneous neural and optical chronic manipulations in freely moving mice. (**a**) Isometric view of the 3D model structure showing the three printable pieces that assemble the implant: a modified version of the flexDrive mechanism (Voigts J, Siegle JH, Pritchett DL and Moore CI (2013). The flexDrive: An ultra-light implant for optical control and highly parallel chronic recording of neuronal ensembles in freely moving mice. Front. Syst. Neurosci. 7:8. DOI: 10.3389/fnsys.2013.00008 open-ephys.org), the lower protection cone and the removable cap. (**b**) Picture taken two months after surgery of a 9-month-old mouse implanted with our custom-built chronic device and using the removable cap. (**c**) Closed-view of "in use" chronic device showing connections for simultaneous recording of electrophysiology activity and optogenetic stimulation. (**d**) Bilateral optic fibers were fixed to reach 2-2.2 mm depth in the dorsomedial striatum. (**e**) The configurable 3D printed driving mechanism targets multiple brain regions. This mechanism was used to move up or down individual tetrodes to chase *in-vivo* for PV interneurons in the CMS while the animal was freely moving.

EXTENDED FIGURE 3.

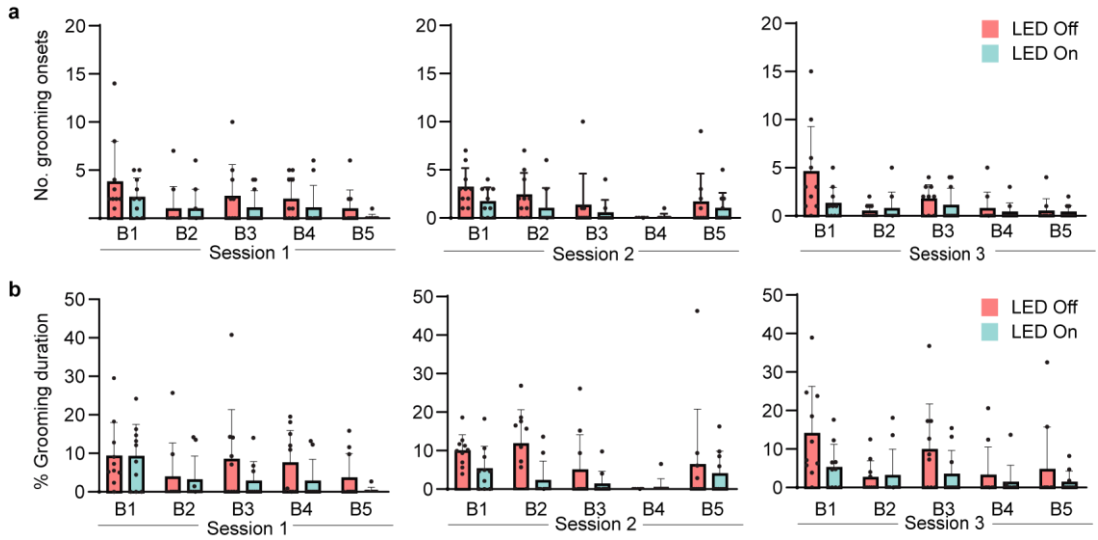

Extended Data Figure 3. Inter-session effect of centro-medial striatal PV interneurons activation in reducing compulsive-like behaviour in Sapap3-PVCre mice. Close-view of (**a**) the number of grooming onsets and (**b**) the percentage of grooming duration for three separated sessions. Each session was completed on different days and included five repetitions (T1-T5) of optogenetic simulation off-on (3 min blocks each) delivered into the CMS of Sapap3-PVCre (n=10).

EXTENDED FIGURE 4.

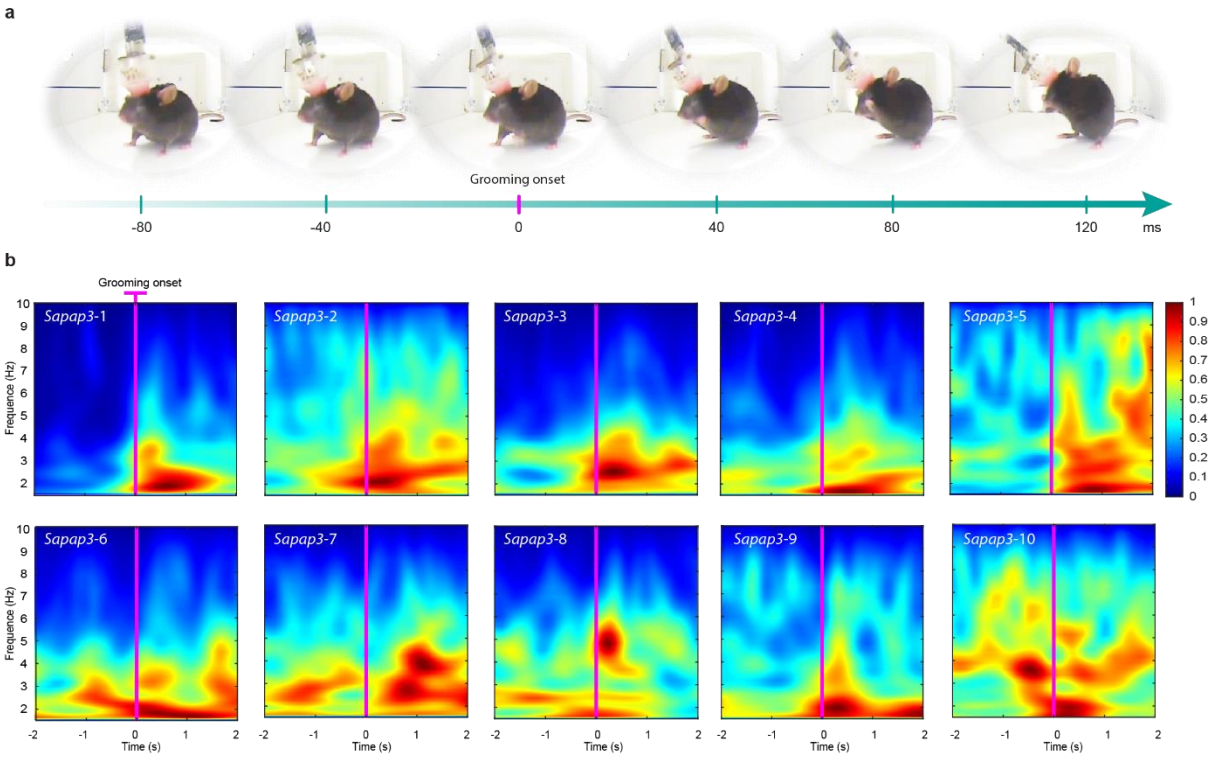

Extended Data Figure 4. Low-frequency LFP signature in the OFC predicts grooming onset. (**a**) Example of consecutive image frames displaying how the grooming onset was assigned to the first frame showing locomotion from anterior limbs to engage in a grooming bout. (**b**) Close-view of an animal-by-animal time-frequency wavelet spectrogram around grooming onset reveals an increase in low-frequency oscillations (inferior to 5Hz) for the assembly of animals. Vertical magenta lines in each spectrogram indicates grooming onset. Each spectrogram represents the averaged LFP normalised activity of grooming events (mean=25 events, SD ±5.25) for a single mouse extracted over different recording sessions (n=10 in Sapap3$^{-/-}$ mice, warmer colours represent higher energy).

EXTENDED FIGURE 5.

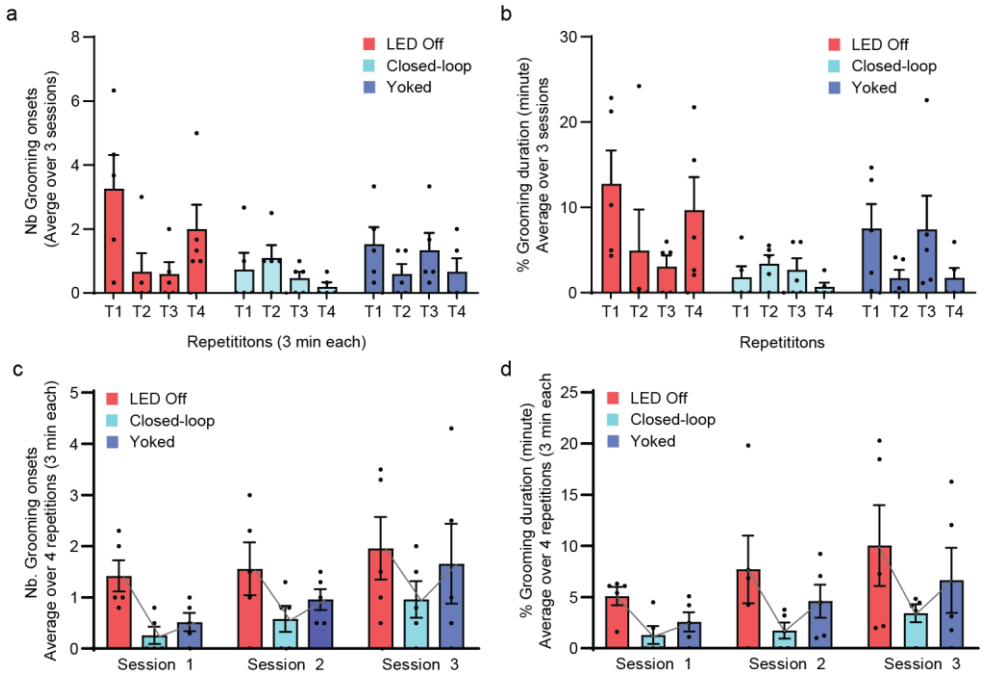

Extended Data Figure 5. Intra-session and inter-session effect comparison of closed-loop stimulation of CMS PV interneurons in reducing compulsive-like behaviour in Sapap3-PVCre mice. Close-view of individual experimental sessions showing all four repetitions for the different conditions: without stimulation, stimulation executed following online prediction of grooming activity and a yoked protocol for (**a**) number of grooming onsets and (**b**) percentage of duration over time. The effect of the three conditions for stimulation delivery over time (for three independent sessions) is shown in (**c**) for the number of grooming onsets and for (**d**) the percentage of grooming duration. N=5 Sapap3-PVCre mice. Error bars represent mean ±SEM.

EXTENDED FIGURE 6.

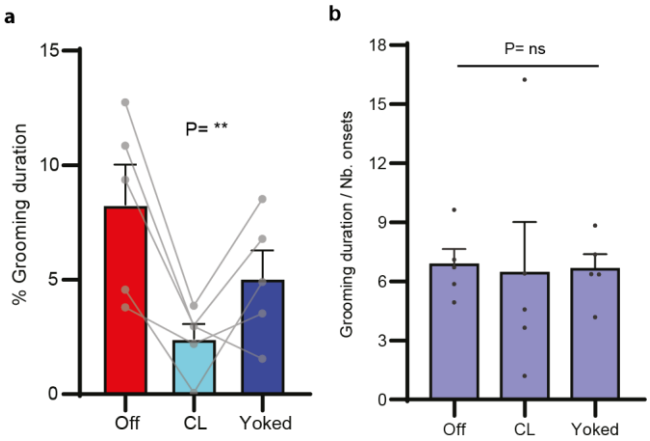

Extended Data Figure 6. Closed-loop optogenetic effect on the total time spent in grooming and the duration of individual grooming bouts. (**a**) The average % of grooming duration during the three different experimental conditions shows that there is a statistically significant trend of lower grooming duration within the closed-loop condition (Jonckheere-Terpstra test for non-parametric trend analysis for ordered alternatives from 'closed-loop', 'yoked' to 'laser-off' condition, T_{JT}= 2.78, **P ≤ 0.01). (**b**) The optogenetics stimulation did not affect the average duration of individual grooming events in either the 'closed-loop', the 'yoked' or the 'laser-off' condition (Repeated measures one-way ANOVA, F= 0.02, P=0.9). N=5 Sapap3-PVCre mice. Error bars represent mean ±SEM.

METHODS

Mice

All experimental procedures have been approved by the French Ministry of Higher Education, Research and Innovation (APAFIS #1418-2015120217347265 and #31141-2021042017105235). Mice were maintained in a 12-hour light/dark cycle with *ad libitum* food and water. The Sapap3-knockout (Sapap3$^{-/-}$) mouse line was provided by Drs. G. Feng and A.M. Graybiel (Massachusetts Institute of Technology, Cambridge, U.S.A.) (B6.129-*Dlgap3*^{tm1Gfng}/J ; Jackson Laboratory stock #008733). *Sapap3*$^{+/-}$ were crossed with parvalbumin (P.V.) (*Pvalb*)-Cre line (B6;129P2-*Pvalb*$^{tm1(cre)Arbr}$/J; Jackson Laboratory stock #008069; provided by Dr A. Bacci, Paris Brain Institute, France) to obtain Cre-positive *Sapap3*$^{+/+}$ and Sapap3$^{-/-}$ mice. Biopsies for genotyping were taken during weaning and at the end of all experimental procedures to verify the absence or presence of the Sapap3 and Cre-recombinase proteins, respectively, according to genotyping recommendations of the Jackson Laboratory (standard PCR assay protocols #24678 and #27783 for PV-Cre and Sapap3$^{-/-}$ line, respectively). For experimental procedures, we used 17 male Sapap3$^{-/-}$ :: PV-$^{Cre/wt}$ (average initial age = 8.6 ±1.4 months, average weight = 30.5 ±3.7 g) and 5 age-matched Sapap3$^{+/+}$::PV-$^{Cre/wt}$ (average initial age = 9.1 ±1 months, average weight = 39.3 ±4 g).

Viral Vectors

Viral vectors expressing either an excitatory opsin and a fluorophore reporter (AAV5-hEF1a-dlox-hChR2(134R)_mCherry(rev)-dlox-WPREhGHpA) or a fluorophore reporter only (AAV5-hSyn1-dlox-mCherry(rev)-dlox-WPRE-hGHpA) were purchased from the Viral Vector facilities of the Neuroscience Center Zurich (University of Zurich and ETH Zurich) and from Addgene Viral Service facilities. Viral vectors were generated from Addgene plasmids #20297 and #50459 and titers determined via fluorometric quantification (Neuroscience Center Zurich) or by real-time quantitative PCR combined with SYBR green technology (Addgene). Respective titers were >9.1x10^{12} vector genomes/ml (Neuroscience Center Zurich, opsin construct), >1.3x10^{13} vector genomes/ml (Neuroscience Center Zurich, control construct) and 1.4 × 10^{13} GC⁄mL (Addgene, opsin construct). The viral vectors were aliquoted and stored at -80°C until stereotaxic injection surgeries.

Headframe implant

Homemade implants were designed and constructed around a transparent plastic core, a modified version of the Open Ephy's flexdrive[42] (Extended Data Figure 2a). The implant was designed with SolidWorks 3D CAD software (Dassault Systems SolidWorks Corporation, MA, U.S.A) and printed via stereolithography using the 3D printer Form2 (Formlabs, Somerville, MA, U.S.A) with clear resin. The plastic drive body core held eight independently mobile tetrodes and two fixed flat optic fiber stubs (Plexon Inc., Texas, U.S.A.) of 200/230 µm (core/core + cladding) inserted in a zirconia ferrule (Extended Data Figure 2c-e). Tetrodes were made from 17.78 µm (0.0007 inches) Formvar-coated nichrome wire (A-M Systems, WA, U.S.A), twisted (Tetrode Assembly Station, Neuralynx, MT, U.S.A), and heated to form tetrodes. Tetrodes were fixed to laser-cut plastic springs (polyethylene terephthalate, 25 mm

from Weber Metaux, Paris, France) and individually driven via miniature screws (0.7M Micro-modele, Strasbourg, France). Electrodes were attached to an electrode interface board (Open Ephys Production Site, Lisbon, Portugal) with gold pins (Neuralynx, MT, U.S.A). Individual electrodes were gold plated to an impedance of 200-350 kΩ. Ground connections were made using 50.8 µm (0.002 inches) Formvar-coated tungsten wires (A-M Systems, WA, U.S.A). The fully assembled implant (drive body, cap, and cone) weighed less than 3 g.

Surgical procedures.

Each mouse received an injection of analgesics (buprenorphine 0.1mg/kg; s.c.) 30 minutes prior to deep anaesthesia (induction at 2.5% % isoflurane; maintenance during surgery at 0.9-1.2% isoflurane). The animals were gently mounted into a digitally equipped stereotaxic frame (David Kopf Instruments) via ear bars adapted for mouse stereotaxic surgeries. The animal's temperature was maintained at 37°C through a heating pad coupled to an anal sonde. Scalp hair was removed using depilation cream (Veet) diluted with sterile 0.9% saline, and the skin was disinfected three times with 70% ethanol and betadine solution (Vétédine, Vétoquinol) before skin incision. Skull and skin were maintained humid during the entire surgery using sterile 0.9% saline. Four small burr holes were drilled around the perimeter of the exposed skull surface to accept steel anchor screws. Two additional small burr holes were drilled behind the estimated implant volume to insert two separate ground wires. For all mice, craniotomies and durotomies (1.0mm diameter) were made bilaterally above the dorsomedial striatum (AP = +1.0 mm, ML = +1.5 mm); for mice with *in-vivo* tetrode recordings in the orbitofrontal cortex (OFC), an additional cranio-/durotomy (0.8mm diameter) was performed above the left lateral orbitofrontal cortex (AP = +2.8 mm, ML = +1.5 mm). Brain surface was maintained humid with sterile 0.9% saline throughout viral injections until headframe implantation. AAV constructs were injected bilaterally at a constant rate of 50nl/min (0.4µl/site) into the dorsomedial striatum (DV -2.4, measured from brain surface) using a motorized micropump (Legato 130, K.D. Scientific) with a precision syringe (Hamilton Gastight Series #1701, 10µl) and respective needles (Hamilton, 33Ga, beveled end). Before virus injection, the needle was lowered to DV = -2.5 mm and retracted to DV = -2.4 mm immediately, where the needle was allowed to settle for 2 minutes. After injections, the needle was maintained in the same position for 10 minutes, then retracted by 300µm (DV = -2.1) and maintained at that position for another minute. Afterwards, the needle was slowly removed from the brain. After each injection, to exclude needle clogging during intracranial procedures, correct flux was tested by visually checking the continuous formation of a droplet using the same injection speed as during intracranial injections. A drop of surgical lubricant was applied to each cranial opening. The implant was carefully lowered so that the bottom polyamide tubes containing either tetrodes or smaller tubing to hold the optic fibers touched the brain surface. The implant was fixed to the skull and screws with dental acrylic (Jet Denture Repair, Fibred Pink powder + liquid, Lang Dental). Ground wires were formed into tiny loops inserted below the skull to make surface contact with the brain. Ground wires were then fixed to the implant frame and connected to the electrode interface board (EIB). Optic fibers were carefully lowered to the depth of 2mm into the brain and glued into position in the opening provided in the EIB. Tetrodes were advanced individually directly after surgery in the orbitofrontal cortex (DV = 1.0 mm) or the striatum (DV = 1.5 - 2 mm) during the following 3-5

postoperative days. A protective 3D-printed cap was screwed to the implant to keep out bedding debris. Animals were injected with analgesics (buprenorphine, 0.1mg/kg; s.c.) directly after surgery and every 12 hours post-surgery on the following day; they were closely monitored until awake in a heating chamber set to 37°C. Animals were then placed into a clean homecage equipped with materials adapted for implanted animals (e.g. no hanging food grids to avoid bumping of the implant). Animals were closely monitored post-surgery twice a day, including veterinary care, taking into account changes in weight, body score, nesting, and overall locomotor activity as indicators of surgery recovery.

Experimental setup

The experimental setup consisted of a homemade arena (290 x 270 mm), in which the mouse was allowed to move freely. The setup structure included passive commutators for electrophysiology and optic stimulation, synchronization L.E.D.s, and two cameras (704x576 resolution; 25 frames per second) installed at opposite walls to allow for complementary views. After surgical recovery, the animals were habituated for three days to human handling, to the electrophysiology acquisition system and the fiber patch cable tethering. The animals were left in the arena with *ad-libitum* food and water for two nights (6 pm to 8 am) of additional habituation to the setup. At the beginning of each experimental session, the mice were carefully tethered and habituated to the arena for 10-15 minutes. Any noises and vibrations were avoided during experimentation. No water or food was provided during the experimental sessions. After each experiment, the behavioural apparatus was cleaned using a disinfectant cleaning spray containing 55% ethanol, washed with soap and water, and dried.

Behavioural assessment.

Manuel scoring was performed using a freely available video scoring software (Kinovea, 0.8.15, www.kinovea.org). Self-grooming activity was assessed by quantifying duration, number of grooming events, and the percentage of grooming time. Grooming onset was defined when the mouse started lifting its front paws to groom. End of grooming was defined as the time point when the mouse stopped grooming for at least one second or when the grooming behaviour was interrupted by another behaviour. We discarded grooming-like phases of less than a second duration. We annotated other behaviours such as, e.g., walking, rearing, sniffing, resting, stretching, heading up, or freezing. The neural activity during these behaviours was used to form a database for our supervised learning algorithm. We scored resting behaviours for the local field potential analysis; these were defined as behavioural activity without major head movements. Hereby the head position was either laying on the floor or lifted as a relaxed, horizontal extension of the spine. The four limbs touched the ground, and the mouse showed a relaxed posture. I.e. no hunched posture or exaggerated respiration as observed for freezing behaviour was stated; ears were not pulled back, and eyes normally opened, not squinted as observed during distress.

Optogenetics

Bilateral optogenetic neuromodulation in the dorsomedial striatum was conducted at least two weeks after stereotaxic viral injections to allow for sufficient recovery and viral expression. The implanted striatal fiber stubs were connected to optical patch cables (200-µm core and 0.5 m length with 0.66 numerical aperture) via mating ferrules in a zirconia sleeve. Optical patch cables were connected to blue light L.E.D. source modules (465 nm) mounted on magnetic L.E.D. commutators. The light stimulation patterns were pre-programmed using Radiant Software (Plexon Inc.). Before experimentation, the output power was measured from the optical fiber tips with a light power meter (Thorlabs PM100D with S120C sensor) and calibrated to 10 mW. Unless otherwise stated, all devices for optogenetic modulations were purchased from Plexon Inc. (Texas, U.S.A).

Continuous optogenetic stimulation. Each experimental session lasted 30 minutes and included ten interleaved OFF (no light stimulation) and ten ON trials (light stimulation of 10mW during 5ms at pulses of 20Hz) of three minutes each.

Closed-loop optogenetic stimulation. Each experimental session lasted 36 minutes. In four repetitive cycles, we alternated OFF trials, trials with closed-loop stimulation (CL), and with yoked stimulation (Y), each lasting 3 minutes. For the CL trials, a custom Matlab (R2017b) algorithm triggered the light stimulation on-demand. Each activation lasted four seconds (10 mW, 5-ms pulses at 20 Hz). In a Y trial, the same number of stimulations delivered in the previous CL trial were pre-assigned randomly (*rand* function) by the algorithm.

Data acquisition and analyses

Electrophysiology. We performed extracellular recordings in awake, freely moving mice using tetrodes attached to a 32-channel connector in a mechanically adjustable drive. All signals were amplified, multiplexed and digitalized at a sampling frequency of 20 kHz using the Intan hardware acquisition system (RHD2000 USB Interface Board with the RHD 32-Channel Headstage, Intan Technologies, CA, U.S.A) and either Intan Software (RHD USB Interface Board software) or Open Ephys G.U.I.[43]. Recordings were analyzed offline. For the closed-loop experiments, we used a custom Matlab code to record with Intan Libraries. A blinking L.E.D. together with a digital input activated simultaneously were used to synchronize video and extracellular recordings.

Local field potential analysis. Neural signals were synchronized with video recordings via TTL signals for local field potential recordings. The spectral content of the L.F.P. signals was analyzed using custom Matlab routines, the Chronux[44] Matlab package (http://chronux.org) and the Matlab Signal Processing toolbox. For Figure 2 and Extended Data Figure 4, we decreased the broadband data sample rate by a factor of 40, and then low-pass filtered the data using a 10th-order Butterworth filter with a cut off frequency of 10 Hz. We performed continuous wavelet transformation around grooming events (4s before and after the onset). We used the Morse wavelet with asymmetry parameter (γ) equal to 3 and a time-bandwidth product equal to 60.

Spike analysis. Spike sorting was performed offline using the valley-seeking prevalent method in Offline sorter (Version 3.3.5, Plexon Inc.), followed by visual screening. Hereby, each set of spike cluster was compared for cross-correlogram features and spike waveform. The spikes of each putative unit were assessed qualitatively regarding ISI-waveform, spike amplitude and waveform consistency. To quantify the effect of light, we used NeuroExplorer (Version 4, Nex

Technologies, Colorado, USA.) rate histogram to display the firing rate versus time with a bin size of 0.05s

Feature selection and supervised learning algorithm

To obtain the predictive value of low-frequency L.F.P. components in the OFC related to the animal's behavioural state ("pre-grooming" and "other behaviour"), we implemented a supervised machine learning classification algorithm. The feed-forward artificial neural network had two output classes, for 'pre-grooming' and 'other behaviour'. We created a database of pre-grooming events and other behaviours for each mouse to train the algorithm. These databases were created from five recording sessions (40 min each), each containing a minimum of 100 events. The database was randomly split into a training data set (70%) and a test dataset (30%). Each electrode was processed individually. We set a threshold policy to decide if the output values of the neural network corresponded to a pre-grooming event or not; only if more than 50% of these detections pointed to a pre-grooming event, it was counted as such. To test the algorithm's performance, we computed the offline recall, accuracy, precision, and specificity for each Sapap3-PVCre mouse tested (n=5).

Histology

After experimental procedures, electrolytic mark lesions were made to confirm the localization of tetrode recording sites. Animals were anesthetized as described above and 5µA constant current was delivered to each electrode during 20 s using an isolated current stimulator (DS3, Digitimer Ltd, Hertfordshire, England). After 72 hours, mice were anesthetized via an intraperitoneal injection of pentobarbital (200mg/kg) and transcardially perfused with 30 ml of 4°C cold 0.9% sodium chloride solution, followed by 60ml of 4°C cold 4% PFA in 1xPBS. Brains were post-fixed in the same paraformaldehyde solution over night at 4°C, briefly rinsed three times in 1xPBS, and progressively dehydrated for cryosectioning by incubations in 15% and subsequently in 30% sucrose solution in 1xPBS for 24 and 48 hours, respectively. Next, brains were embedded in O.C.T. compound and sectioned into six series of 40µm coronal sections (Microm HM N°560, Thermo Scientific) into 1xPBS containing 0.1% sodium azide. Prefrontal sections were stained with a freshly filtered, 1% cresyl violet solution and analyzed for the location of the mark lesions under a brightfield microscope. Immunofluorescence stainings were performed on the striatal sections of one series in 4°C cold solutions on an orbital shaker. Concretely, sections were washed three times for ten minutes in 1xPBS, followed by three washes of each ten minutes in 1x PBS containing 0.1% Tween 20 and 0.2% Triton-X. Sections were next blocked for two hours in 5% normal goat serum in 1xPBS containing 0.1% Tween 20 and 0.2% Triton-X. Subsequently, sections were incubated in the same blocking buffer containing anti-red fluorescent protein antibody (polyclonal anti-RFP, Rockland, #600-401-379, Lot #35634; dilution: 1:1000) on an orbital shaker at 4°C overnight. Sections were then washed three times for ten minutes in 1xPBS with 0.1% Tween 20 and 0.2% Triton-X and incubated for two hours in a blocking buffer containing a secondary antibody (polyclonal anti-rabbit Cy3-conjugated AffiniPure, produced in goat, Lot 106489; dilution 1:400). Afterward, sections were washed twice for ten minutes in 1xPBS with 0.1% Tween 20 and 0.2% Triton-X, followed by one washing for ten minutes in 1xPBS. Sections were next incubated for 2 minutes and 30 seconds in DAPI solution (10µg/ml), washed three

times for ten minutes in 1xPBS, mounted in 0.1M phosphate buffer onto Superfrost Plus slides and coverslipped using fluorescence-protecting medium (FluoromountTM, Sigma Aldrich). A selection of sections was incubated in the same buffer with an additional anti-parvalbumin antibody (polyclonal anti-PV GP 72, Swant, dilution 1:5000) in order to verify viral infection of specifically parvalbumin-positive cells. The secondary antibody solution additionally contained polyclonal anti-goat Alexa488, produced in goat (Invitrogen, Lot #145863, dilution: 1:400). All striatal sections were imaged using a slide scanner (Axio Scan.Z1, ZEISS) and the sections were analyzed and mapped using ZEN software (ZEISS) and a mouse brain atlas[45].

Statistical analysis.

We used Prism (Version 8.0.1, GraphPad Software Inc) to perform the following statistical analyses: Wilcoxon matched-pairs signed-rank test (Paired, non-parametric test, two-tailed, confidence level 95%), Mann Whitney test (Unpaired, non-parametric test, comparing ranks, two-tailed, confidence level 95%), and repeated measures one-way ANOVA (not assuming sphericity, using the Geisser-Greenhouse correction). Statistical significance for the trend analysis for ordered alternatives was assessed using the Jonckheere-Terpstra test performed using the Matlab function from Cardillo G. (2008) Jonckheere-Terpstra test: A non-parametric test for Trend (http://www.mathworks.com/matlabcentral/fileexchange/22159).

Data availability

The data that support the findings of this study are available from the corresponding author upon reasonable request

Code availability

The custom code for the LFP analysis that supports the findings of this study are available from the corresponding author upon reasonable request. The custom code for the feature selection and supervised learning algorithm is at the moment not available for sharing due to ongoing patent submission process.

REFERENCES

1. Gunaydin, L. A. & Kreitzer, A. C. Cortico-Basal Ganglia Circuit Function in Psychiatric Disease. *Annu. Rev. Physiol.* **78**, 327–350 (2016).
2. Corbit, L. H., Nie, H. & Janak, P. H. Habitual alcohol seeking: time course and the contribution of subregions of the dorsal striatum. *Biol. Psychiatry* **72**, 389–395 (2012).
3. Chamberlain, S. R. *et al.* Orbitofrontal dysfunction in patients with obsessive-compulsive disorder and their unaffected relatives. *Science* **321**, 421–422 (2008).
4. Anticevic, A. *et al.* Global resting-state functional magnetic resonance imaging analysis identifies frontal cortex, striatal, and cerebellar dysconnectivity in obsessive-compulsive disorder. *Biol. Psychiatry* **75**, 595–605 (2014).
5. Joel, D., Doljansky, J. & Schiller, D. 'Compulsive' lever pressing in rats is enhanced following lesions to the orbital cortex, but not to the basolateral nucleus of the amygdala or to the dorsal medial prefrontal cortex. *Eur. J. Neurosci.* **21**, 2252–2262 (2005).
6. Burguière, E., Monteiro, P., Feng, G. & Graybiel, A. M. Optogenetic stimulation of lateral orbitofronto-striatal pathway suppresses compulsive behaviors. *Science* **340**, 1243–1246 (2013).
7. Davis, G. L. *et al.* Ketamine increases activity of a fronto-striatal projection that regulates compulsive behavior in SAPAP3 knockout mice. *Nat. Commun.* **12**, 6040 (2021).
8. Saxena, S., Brody, A. L., Schwartz, J. M. & Baxter, L. R. Neuroimaging and frontal-subcortical circuitry in obsessive-compulsive disorder. *Br. J. Psychiatry* **173**, 26–37 (1998).
9. Ramírez-Armenta, K. I. *et al.* Optogenetic inhibition of indirect pathway neurons in the dorsomedial striatum reduces excessive grooming in Sapap3-knockout mice. *Neuropsychopharmacol. Off. Publ. Am. Coll. Neuropsychopharmacol.* **47**, 477–487 (2022).
10. Baxter, L. R. *et al.* Caudate glucose metabolic rate changes with both drug and behavior therapy for obsessive-compulsive disorder. *Arch. Gen. Psychiatry* **49**, 681–689 (1992).

11. Bijanki, K. R. *et al.* Defining functional brain networks underlying obsessive-compulsive disorder (OCD) using treatment-induced neuroimaging changes: a systematic review of the literature. *J. Neurol. Neurosurg. Psychiatry* **92**, 776–786 (2021).

12. Gittis, A. H., Nelson, A. B., Thwin, M. T., Palop, J. J. & Kreitzer, A. C. Distinct Roles of GABAergic Interneurons in the Regulation of Striatal Output Pathways. *J. Neurosci.* **30**, 2223–2234 (2010).

13. Mallet, N., Moine, C. L., Charpier, S. & Gonon, F. Feedforward Inhibition of Projection Neurons by Fast-Spiking GABA Interneurons in the Rat Striatum In Vivo. *J. Neurosci.* **25**, 3857–3869 (2005).

14. Planert, H., Szydlowski, S. N., Hjorth, J. J. J., Grillner, S. & Silberberg, G. Dynamics of Synaptic Transmission between Fast-Spiking Interneurons and Striatal Projection Neurons of the Direct and Indirect Pathways. *J. Neurosci.* **30**, 3499–3507 (2010).

15. Silberberg, G. & Bolam, J. P. Local and afferent synaptic pathways in the striatal microcircuitry. *Curr. Opin. Neurobiol.* **33**, 182–187 (2015).

16. K, L. *et al.* Parvalbumin Interneurons Modulate Striatal Output and Enhance Performance during Associative Learning. *Neuron* **93**, (2017).

17. O'Hare, J. K. *et al.* Striatal fast-spiking interneurons selectively modulate circuit output and are required for habitual behavior. *eLife* **6**, e26231 (2017).

18. Owen, S. F., Berke, J. D. & Kreitzer, A. C. Fast-Spiking Interneurons Supply Feedforward Control of Bursting, Calcium, and Plasticity for Efficient Learning. *Cell* **172**, 683-695.e15 (2018).

19. Burguière, E., Monteiro, P., Mallet, L., Feng, G. & Graybiel, A. M. Striatal circuits, habits, and implications for obsessive-compulsive disorder. *Curr. Opin. Neurobiol.* **30**, 59–65 (2015).

20. Kataoka, Y. *et al.* Decreased number of parvalbumin and cholinergic interneurons in the striatum of individuals with Tourette syndrome. *J. Comp. Neurol.* **518**, 277–291 (2010).

21. Kalanithi, P. S. A. *et al.* Altered parvalbumin-positive neuron distribution in basal ganglia of individuals with Tourette syndrome. *Proc. Natl. Acad. Sci. U. S. A.* **102**, 13307–13312 (2005).

22. Briones, B. A. *et al.* Perineuronal nets in the dorsomedial striatum contribute to behavioral dysfunction in mouse models of excessive repetitive behavior. *Biol. Psychiatry Glob. Open Sci.* (2021) doi:10.1016/j.bpsgos.2021.11.005.

23. Welch, J. M. *et al.* Cortico-striatal synaptic defects and OCD-like behaviours in Sapap3-mutant mice. *Nature* **448**, 894–900 (2007).

24. Rotge, J.-Y. *et al.* Meta-analysis of brain volume changes in obsessive-compulsive disorder. *Biol. Psychiatry* **65**, 75–83 (2009).

25. Rotge, J.-Y. *et al.* Gray matter alterations in obsessive-compulsive disorder: an anatomic likelihood estimation meta-analysis. *Neuropsychopharmacol. Off. Publ. Am. Coll. Neuropsychopharmacol.* **35**, 686–691 (2010).

26. Simon, D., Kaufmann, C., Müsch, K., Kischkel, E. & Kathmann, N. Fronto-striato-limbic hyperactivation in obsessive-compulsive disorder during individually tailored symptom provocation. *Psychophysiology* **47**, 728–738 (2010).

27. Lei, H., Lai, J., Sun, X., Xu, Q. & Feng, G. Lateral orbitofrontal dysfunction in the Sapap3 knockout mouse model of obsessive–compulsive disorder. *J. Psychiatry Neurosci. JPN* **44**, 120–131 (2019).

28. Manning, E. E., Geramita, M. A., Piantadosi, S. C., Pierson, J. L. & Ahmari, S. E. Distinct patterns of abnormal lateral orbitofrontal cortex activity during compulsive grooming and reversal learning normalize after fluoxetine. *Biol. Psychiatry* (2021) doi:10.1016/j.biopsych.2021.11.018.

29. Gage, G. J., Stoetzner, C. R., Wiltschko, A. B. & Berke, J. D. Selective activation of striatal fast-spiking interneurons during choice execution. *Neuron* **67**, 466–479 (2010).

30. Lee, K. *et al.* Parvalbumin Interneurons Modulate Striatal Output and Enhance Performance during Associative Learning. *Neuron* **93**, 1451-1463.e4 (2017).

31. Martiros, N., Burgess, A. A. & Graybiel, A. M. Inversely Active Striatal Projection Neurons and Interneurons Selectively Delimit Useful Behavioral Sequences. *Curr. Biol. CB* **28**, 560-573.e5 (2018).

32. Corbit, V. L., Manning, E. E., Gittis, A. H. & Ahmari, S. E. Strengthened Inputs from Secondary Motor Cortex to Striatum in a Mouse Model of Compulsive Behavior. *J. Neurosci. Off. J. Soc. Neurosci.* **39**, 2965–2975 (2019).

33. Dejean, C. *et al.* Prefrontal neuronal assemblies temporally control fear behaviour. *Nature* **535**, 420–424 (2016).

34. Karalis, N. *et al.* 4-Hz oscillations synchronize prefrontal-amygdala circuits during fear behavior. *Nat. Neurosci.* **19**, 605–612 (2016).

35. Provenza, N. R. *et al.* Long-term ecological assessment of intracranial electrophysiology synchronized to behavioral markers in obsessive-compulsive disorder. *Nat. Med.* **27**, 2154–2164 (2021).

36. Nuttin, B., Cosyns, P., Demeulemeester, H., Gybels, J. & Meyerson, B. Electrical stimulation in anterior limbs of internal capsules in patients with obsessive-compulsive disorder. *Lancet Lond. Engl.* **354**, 1526 (1999).

37. Mallet, L. *et al.* Subthalamic nucleus stimulation in severe obsessive-compulsive disorder. *N. Engl. J. Med.* **359**, 2121–2134 (2008).

38. N, L. *et al.* A Unified Functional Network Target for Deep Brain Stimulation in Obsessive-Compulsive Disorder. *Biol. Psychiatry* **90**, (2021).

39. Spix, T. A. *et al.* Population-specific neuromodulation prolongs therapeutic benefits of deep brain stimulation. *Science* **374**, 201–206 (2021).

40. Zrenner, C., Belardinelli, P., Müller-Dahlhaus, F. & Ziemann, U. Closed-Loop Neuroscience and Non-Invasive Brain Stimulation: A Tale of Two Loops. *Front. Cell. Neurosci.* **10**, 92 (2016).

41. Ghasemi, P., Sahraee, T. & Mohammadi, A. Closed- and Open-loop Deep Brain Stimulation: Methods, Challenges, Current and Future Aspects. *J. Biomed. Phys. Eng.* **8**, 209–216 (2018).

42. Voigts, J., Siegle, J. H., Pritchett, D. L. & Moore, C. I. The flexDrive: an ultra-light implant for optical control and highly parallel chronic recording of neuronal ensembles in freely moving mice. *Front. Syst. Neurosci.* **7**, 8 (2013).

43. Siegle, J. H. *et al.* Open Ephys: an open-source, plugin-based platform for multichannel electrophysiology. *J. Neural Eng.* **14**, 045003 (2017).

44. Mitra, P. & Bokil, H. *Observed Brain Dynamics*. (Oxford University Press, 2008).

45. Paxinos, G. & B. J. Franklin, K. *The Mouse Brain in Stereotaxic Coordinates*. vol. 1 (Academic Press, 2001).